

Combustion Characteristics of Coal for Pulverized Coal Injection (PCI) Blending with Steel Plant Flying Dust and Waste Oil Sludge

Yu Wang, Chong Zou,* Junxue Zhao, and Fei Wang

Cite This: *ACS Omega* 2021, 6, 28548–28560

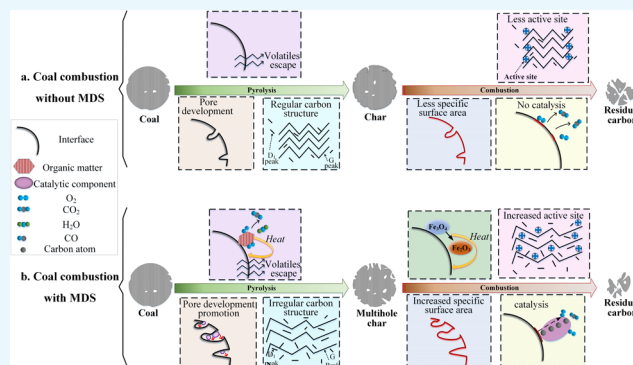
Read Online

ACCESS |

Metrics & More

Article Recommendations

ABSTRACT: Various characterization methods are used to investigate the physical and chemical properties of steel plant flying dust and waste oil sludge, and the combustion characteristics of the mixtures with pulverized coal are studied via thermogravimetric analysis; the catalytic combustion mechanism is also explored. The results show that two types of metallurgical by-products with small particle sizes and developed pores are evenly dispersed in the pulverized coal and are stably combined with it. The additives reduce the ignition temperature and the temperature corresponding to the maximum combustion rate of pulverized coal; simultaneously, they increase the heat released during pulverized coal combustion. During the pyrolysis stage of pulverized coal, the heat generated via organic component combustion in waste oil sludge promotes a cracking reaction and improves the development of the char's micropore. During the char combustion stage, no catalyst deactivation phenomenon occurs under the ratios of inorganic components in the two types of metallurgical dust and sludge. Two additives markedly reduce the activation energy of the combustion reaction.



1. INTRODUCTION

Being one of the most primary solid waste emissions in the steel production process, metallurgical dust and sludge (MDS) are primarily produced in dry or wet dust collection and metallurgical wastewater treatment systems.¹ In 2020, the output of MDS in China reached ~110 million tons, and most of this output has currently been returned to the iron ore agglomeration process. Owing to the characteristics of fine powder, complex composition, and large differences in the components of MDS, they negatively impact the metallurgical properties of sinter and pellet.²

In the pulverized coal injection (PCI) process of a blast furnace (BF), intensifying the combustion of pulverized coal in the raceway and tuyere is the key to increasing the injection ratio.^{3,4} In addition to widely used technologies that cooperate with PCI, such as oxygen enrichment and high temperature of hot blast air,^{5,6} the catalytic combustion technology for PCI coal has attracted the attention of metallurgical researchers in recent years.⁷ From the perspective of chemical reactions, adding a suitable quantity of appropriate additives to the PCI coal can reduce the combustion reaction's activation energy, increase the combustion rate, and improve its combustion efficiency. However, there are many constraints on the selection of additives; for example, some materials with an excellent catalytic effect are expensive to use and some will corrode the BF or pollute its products.

Recently, based on the characteristics of MDS, which contain a relatively high ratio of Fe and Ca compounds with catalytic combustion activity, some researchers have proposed the use of MDS as a catalytic additive for PCI.^{8–15} This not only realizes closed-loop absorption of dust and sludge in the metallurgical process but also improves the combustion performance of PCI.⁹ Senk *et al.*¹⁰ verified the feasibility of injecting such metallurgical dust into the BF by simulating the process of dust and pulverized coal being injected into the blast furnace raceway. Ökqvist *et al.*¹¹ found that adding converter slag or BF dust to coal could improve combustion efficiency. Our research shows that among several types of common MDS, converter dust, i.e., steel plant flying dust (SFD), has relatively high catalytic combustion enhancement activity as it contains transition metals and alkaline earth metal compounds.^{12–14} The source of dust, the adding ways, and the ratio of addition significantly affect catalytic activity.¹⁵

Received: May 19, 2021

Accepted: October 1, 2021

Published: October 21, 2021



In the steel production process, there is a special and difficult-to-handle type of MDS, called waste oil sludge (WOS). WOS is a three-phase mixture formed by the combination of waste machine oil generated during the operation of metallurgical process equipment, water, and iron-containing dust. It is a gray-black oil sludge with a pungent odor, designated as a hazardous waste in the Resource Conservation and Recovery Act (RCRT).^{16–18} For every ton of steel produced, 0.86 kg of WOS is estimated to be generated,¹⁹ and the annual output of oil sludge in numerous large steel plants reaches tens of thousands of tons. The current methods of processing oil sludge are mainly as follows: chemical extraction,²⁰ incineration,^{21,22} biodegradation,^{23,24} and pyrolysis.^{25,26} However, most of these methods have problems such as high investment cost, difficult equipment maintenance, low utilization efficiency, and environmental pollution.^{20,27,28} Therefore, a large quantity of WOS has accumulated in steel enterprises over a long period, and this quantity is increasing; such accumulated WOS not only occupies land and pollutes the environment but also wastes resources.²⁹ Similar to SFD, the WOS contains a high ratio of Fe and Ca compounds that possibly generate a catalytic combustion effect; in addition, the organic matter in WOS exhibits good combustion reactivity.²³ Therefore, present work also explores the feasibility of using WOS as a combustion additive of PCI coal.

The composition of MDS is complex and can be treated as a composite additive. Numerous studies^{30–33} have shown that the various components in the composite additive have different effects and mechanisms of action on coal devolatilization and char combustion during the coal combustion process. However, our previous studies have shown that there is a sintering catalytic deactivation phenomenon between the calcium oxide and iron oxide in the dust at a specific ratio and temperature conditions. When the ratio of Fe to Ca is 8:2, Fe₂O₃ and CaO react to form CaO·Fe₂O₃ at temperatures of 700–1000 °C, which gives rise to sintering and reduces the specific surface area of the catalyst. When the ratio of Fe to Ca is 2:8, the formation of 2CaO·Fe₂O₃ at 800–900 °C decreases the rate and efficiency of combustion.³² Avoiding these disadvantages can significantly improve the catalytic effect of the dust.³⁴ To date, the carbon–oxygen reaction mechanism of the catalytic reaction mainly includes the electron transfer theory,³⁵ oxygen transfer theory,³⁶ the spillover mechanism,³⁷ the carbon dissolution mechanism,³⁷ and the bulk diffusion mechanism.³⁸ Of these theories, the bulk diffusion mechanism has received considerable attention as it can explain some phenomena (“channels” and isotope experiment) that cannot be explained by other theories.^{39,40} In this theory, carbon atoms can dissolve at the carbon–catalyst interface and enter its interior, then diffuse in the catalyst, and finally reach the gas–catalyst surface and contact with oxygen molecules adsorbed on the catalyst surface to accelerate the carbon–oxygen reaction.

To improve the combustion performance of PCI coal in the raceway and recycle MDS resources, the effects and mechanism of SFD and WOS on the combustion characteristics of anthracite are studied. First, various characterization methods are adopted to study the basic composition and physical as well as chemical properties of SFD and WOS, focusing on the analysis of the organic composition and thermal decomposition characteristics of WOS; second, the thermogravimetric (TG)-differential scanning calorimetry (DSC) method is used to investigate the influence of MDS in different ratios on the combustion characteristic parameters of pulverized coal; finally,

the influence of additives on the char structure and the interaction between the catalytic components during devolatilization are analyzed, and the changes in the activation energy of pulverized coal combustion before and after adding the additives are compared. Based on the above results, a catalytic combustion mechanism is proposed.

2. EXPERIMENTAL SECTION

2.1. Samples. The fuel sample, anthracite, used herein comes from the PCI workshop of an ironmaking enterprise. The proximate analysis of the coal sample is summarized in Table 1.

Table 1. Proximate Analysis of Anthracite (wt %)

M_{ad}	A_{ad}	V_{ad}	FC_{ad}
0.82	13.20	10.62	75.36

The pulverized coal is ground to less than 74 μm particle size. SFD and WOS are from the dust collection system and the sewage treatment in the converter steelmaking workshop, respectively. The chemical composition is shown in Table 2.

Table 2. Composition of SFD and WOS (wt %)

components	WOS	SFD
organic matter	19.00%	
Fe ₂ O ₃	30.56%	46.84%
CaO	11.03%	23.4%
Na ₂ O	0.54%	1.30%
MgO	2.43%	4.86%
Al ₂ O ₃	13.74%	1.55%
SiO ₂	14.18%	6.51%
P ₂ O ₅	0.44%	0.21%
SO ₃	3.89%	1.35%
K ₂ O	0.20%	1.52%
MnO	0.63%	7.35%
TiO ₂	0.28%	0.24%
ZnO	0.09%	3.30%
BaO	0.00%	0.35%
total	98.02%	98.78%
calorific value	13,581 J/g	

The three samples are placed in a drying oven at 120 °C for 2 h. Because WOS is agglomerated post drying, it becomes a fine powder after being gently ground with a mortar for 10 min. All samples of WOS are stored in a drying vessel for later use. Dissimilarly, WOS used in thermal characteristics investigation did not undergo drying treatment with the purpose of understanding the water release behavior.

The additives and pulverized coal are mechanically mixed by a drum mixer, and the ratios of additives in pulverized coal are 1.0, 1.4, 1.8, 2.2, 2.6, and 3% for various samples. The mixing time is 30 min, and the rotation speed is 270 r/min. The pulverized coal without any added substance is used as a blank sample, and the same mixing procedure is performed. To observe the additives and pulverized coal along with mixing uniformity under scanning electron microscopy (SEM), the graphite powder whose properties are similar to pulverized coal (the average particle size is close to pulverized coal) is adopted as the base mixing substance, and the additives and adding method are the same as above.

Aiming at analyzing the influence of additives on the structure of char, a horizontal tube furnace (BYT, TL1200-I, China) is

adopted to prepare char samples. The raw coal sample after the above treatment and the samples added with a 10% SFD and WOS mixture weigh 5 ± 0.01 g and are placed in a 30×100 mm Al_2O_3 crucible. The resulting sample is heated from room temperature to 200 °C at a rate of 10 °C/min under the condition of a nitrogen flow rate of 500 mL/min, held for 10 min, and then heated to 700 °C at a rate of 10 °C/min, held for 30 min, and cooled to room temperature with the furnace.

2.2. Characterization Methods. The particle size distribution of the additive is measured using the wet method with a laser particle size analyzer (Retsch, Camsizer P4, Germany); the dispersant is deionized water. The element composition of the additive is measured using an X-ray fluorescence spectrometer (Rigaku, ZSX PrimusII, Japan) and converted to the percentage content of oxide. The calorific value of WOS is measured using an automatic touch control microcomputer calorimeter (TianKe, ZDHW-8E, China). The specific surface area and pore distribution of the additives are measured using a physical adsorption analyzer (JWGB Sci. & Tech., Beijing, China). The sample weight is 1.5 g, the degassing temperature is 120 °C, and the degassing time is 2 h. The surface morphology is observed via SEM-electron backscatter diffraction (EBSD) (Oberkochen, Supra55, 168Zeiss, Germany). Samples are dispersed on a conductive stage using the conductive double-sided tape, imaged using the EBSD probe at a working voltage of 20.00 kV and at a working distance of 4.8 mm. The functional group structures of the organic compounds are detected by a Fourier transform infrared (FTIR) spectrometer (Thermo Fisher Scientific, Nicolet iSS, USA), and the sample preparation is performed via the KBr pellet method with a scanning range of 400 – 4000 cm^{-1} . The change in the carbon chemical structure during the pyrolysis of the sample is measured using a laser Raman spectrum microscope (Horiba, LabRAM HR Evolution, France) with a wavelength of 514 nm and a range of 800 – 2000 cm^{-1} .

The effect of additives on the combustion characteristics of pulverized coal is tested on a TG-DSC integrated thermal analyzer (SETARM, Setsys evolution, France); the sample weight is 10 ± 0.1 mg, the carrier gas is pure oxygen (99.99%), the flow rate is 100 mL/min, the heating rate is 15 °C/min, and the heating temperature is 50 °C– 1000 °C. The thermal decomposition characteristics of WOS are also measured through the thermal analysis method.

2.3. Evaluation of Combustion Behavior. The following parameters are adopted to compare the combustion behavior of coal before and after adding additives.

- (1) Ignition temperature T_i : ignition temperature is an important characteristic parameter used to measure the difficulty of fuel ignition, which is obtained by the TG-DTG method.⁴¹
- (2) The temperature corresponding to the maximum combustion rate T_m : It characterizes the temperature when the fuel is combusted intensively. If this temperature is low, the combustion process occurs in advance and the reactivity is better.
- (3) Burnout index D_f : A larger D_f value implies a higher burnout degree of the fuel. It is defined as follows:⁴²

$$D_f = \frac{(dw/dt)_{\max}}{\Delta t_{1/2} t_m t_f} \quad (1)$$

where t_m and t_f are the times corresponding to T_m and T_f , respectively, $\Delta t_{1/2}$ is the time corresponding to the temperature

interval when $(dw/dt)/(dw/dt)_{\max} = 1/2$, and T_f is the burnout temperature (temperature at the burnout rate of 98%).

- (4) The heat quantity ΔQ in the reaction process represents the heat release of the entire combustion process. When this value is higher, the heat release of the entire combustion process is higher and the corresponding catalytic effect is better:

$$\Delta Q = \frac{\int h(t) dt}{m_0(1-x)} = \frac{ks}{m_0(1-x)} \quad (2)$$

where ΔQ is the enthalpy ($\text{kJ} \cdot \text{g}^{-1}$), k is a constant, m_0 is the initial mass of the sample (mg), x is the ratio of the catalyst added (wt %), and S is the peak area enclosed by the DSC curve and the baseline.

2.4. Kinetic Analysis Method. In this study, the Coats–Redfern integration method⁴³ is applied to calculate the kinetic parameters of the combustion reaction. The conversion rate equation is generally described as follows:

$$\frac{d\alpha}{dt} = k(T)f(\alpha) \quad (3)$$

$$k(T) = A \exp\left(-\frac{E}{RT}\right) \quad (4)$$

Here, α is the conversion rate, t is the reaction time (min), $k(T)$ is the rate constant, T is the reaction temperature (K), $f(\alpha)$ is the reaction mechanism function, which can be written as $f(\alpha) = (1-\alpha)^n$, n is the reaction order, A is the pre-exponential factor (s^{-1}), E is the activation energy (kJ/mol), and R is the molar gas constant (8.314 J/(mol k)).

The equation for the conversion rate α is as follows:

$$\alpha = \frac{m_0 - m_t}{m_0 - m_f} \quad (5)$$

Here, m_0 is the initial mass (mg) of the sample, m_t is the final mass (mg) of the sample, and m_f is the mass (mg) of the sample at time t .

The constant heating rate β of the nonisothermal combustion experiment can be expressed as dT/dt . Equations 4 and 5 can be combined into the following equations:

$$\frac{d\alpha}{dT} = \frac{1}{\beta} \frac{d\alpha}{dt} = \frac{1}{\beta} A \exp\left(-\frac{E}{RT}\right) (1-\alpha)^n \quad (6)$$

After obtaining the integrated eq 6, eq 7 can be obtained:⁴⁴

$$\begin{cases} \ln\left[\frac{1-(1-\alpha)}{T^2}\right] = \ln\left[\frac{AR}{\beta E}\left(1-\frac{2RT}{E}\right)\right] - \frac{E}{RT} (n=1) \\ \ln\left[\frac{1-(1-\alpha)^{1-n}}{T^2(1-n)}\right] \\ = \ln\left[\frac{AR}{\beta E}\left(1-\frac{2RT}{E}\right)\right] - \frac{E}{RT} (n \neq 1) \end{cases} \quad (7)$$

For the high temperature range of the combustion process and most E values, $E/RT \geq 1$ and $1-2RT/E \approx 1$. Thus, eq 7 can be further simplified as:

$$\begin{cases} \ln \left[\frac{1 - (1 - \alpha)}{T^2} \right] = \ln \left[\frac{AR}{\beta E} \right] - \frac{E}{RT} (n = 1) \\ \ln \left[\frac{1 - (1 - \alpha)^{1-n}}{T^2(1 - n)} \right] = \ln \left[\frac{AR}{\beta E} \right] - \frac{E}{RT} (n \neq 1) \end{cases} \quad (8)$$

From the slope and intercept of the straight line, the activation energy E and the pre-exponential factor A are obtained.

3. RESULTS AND DISCUSSION

3.1. Properties of MDS. The XRD results of the two types of MDS are shown in Figure 1. Both SFD and WOS contain a

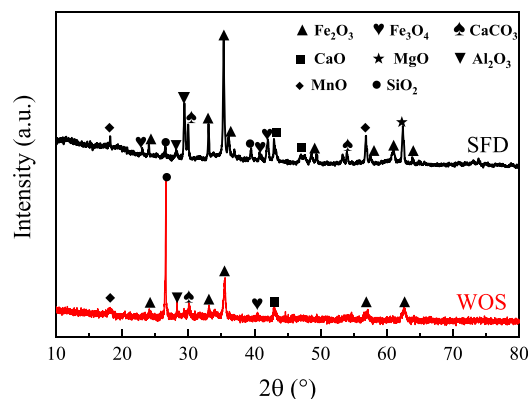


Figure 1. Phase composition of SFD and WOS.

magnetite phase (Fe_3O_4), a hematite phase (Fe_2O_3), a calcite phase (CaCO_3), and a quicklime phase (CaO). The iron oxides in the MDS may be produced by the oxidation of the evaporated molten steel discharged from the converter exhaust system. The calcium compounds in the MDS may originate from slagging elements that regulate the alkalinity of slag. In addition, the two types of dust and sludge also contain Mn, Al, Mg, Si, and other oxide minerals, which may originate from additives that adjust the composition of molten steel.

The particle size distribution of SFD and WOS is shown in Figure 2. The particle size of SFD is in the range of 0.1–1.2 μm , and the average particle size D_{50} is 0.37 μm ; the particle size of WOS is in the range of 0.4–7 μm , and the average particle size D_{50} is 1.12 μm . The particle sizes of the two types of MDS are

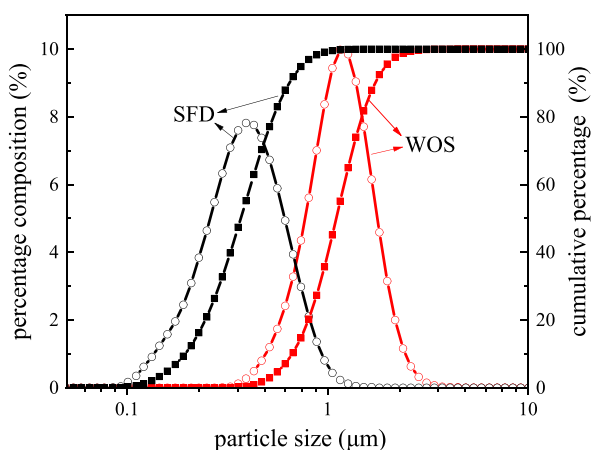


Figure 2. Particle size distribution of SFD and WOS.

smaller than those of the dust and sludge from the common iron and steel metallurgical process.⁴⁵ This indicates that SFD and WOS are more conducive to mixing with coal and there are more contact points after mixing with pulverized coal, which is beneficial for improving the catalytic effect.

The pore volume and pore specific surface area distributions of the two additives are shown in Table 3 and Figure 3. The

Table 3. Pore Structure Parameters of the SFD and WOS Using the N_2 Adsorption Method

sample	specific surface area (m^2/g)	total pore volume (cm^3/g)	average pore size (nm)
SFD	4.654	0.016	9.737
WOS	0.773	0.002	5.365

specific surface area of SFD is 4.654 m^2/g and the average pore size is 9.737 nm, whereas the specific surface area of WOS is 0.773 m^2/g and the average pore size is 5.365 nm. Figure 3a shows that the pore size range of SFD is 3–68 nm and the pore size range of WOS is 3–60 nm, both of which are mainly mesoporous; in contrast, SFD has a larger pore size range. Figure 3b demonstrates that pores below 30 nm in SFD contribute more to the specific surface area, and pores below 28 nm in WOS contribute more to the specific surface area. In contrast, SFD has more developed pores and a larger specific surface area. The pore structure of the catalyst has a greater impact on the catalytic effect. A higher specific surface area will increase the contact area between pulverized coal and the catalyst, thereby promoting the combustion of pulverized coal.⁴¹

As WOS contains about 20% organic compounds, IR analysis is conducted. The obtained results are shown in Figure 4. The three points with wavenumbers of 871.97, 1011.06, and 1635.26 cm^{-1} are the benzene 5 substitution (1H), hydroxy benzene, and hydroxy benzene C=C functional groups. These functional groups will form cycloalkanes and aromatic hydrocarbons. The wavenumber of 1379.22 cm^{-1} is the $-\text{CH}_2$ and C=O functional groups. The wavenumber of 1460 cm^{-1} is the $-\text{CH}_3$ and $-\text{CH}_2$ functional groups. These functional groups are the main components of alkanes. The two functional groups with wavenumbers of 2854.25 and 2924.02 cm^{-1} are the symmetry R_2CH_2 and antisymmetry R_2CH_2 functional groups, respectively; the wavenumber of 3412.26 cm^{-1} is the self-associated hydroxyl. These functional groups are more consistent with those of base oils in lubricating oil, grease, hydraulic oil, and gear oil, including alkanes (straight chain, branched chain, and multibranch chain), cycloalkanes (monocyclic, bicyclic, and polycyclic), aromatics (monocyclic aromatic hydrocarbons and polycyclic aromatic hydrocarbons), cycloalkyl aromatic hydrocarbons, and oxygen-containing, nitrogen-containing, and sulfur-containing organic compounds and non-hydrocarbon compounds such as colloids and asphaltenes.⁴⁶ Therefore, the organic composition of WOS is a common type of machine oil added in some metallurgical equipment.

The TG-DSC curves of the thermal decomposition of WOS in argon and oxygen atmospheres are shown in Figure 5. The thermal decomposition of WOS in an argon atmosphere in Figure 5a can be divided into three stages: water volatilization (below 140 $^\circ\text{C}$), volatile oil volatilization (140–600 $^\circ\text{C}$), and inorganic matter decomposition (above 600 $^\circ\text{C}$). The weight losses of the three processes are 16.24, 20.6, and 6.91%, respectively, and it can be concluded that the water and oil content of the WOS is $\sim 37\%$. The volatilization and

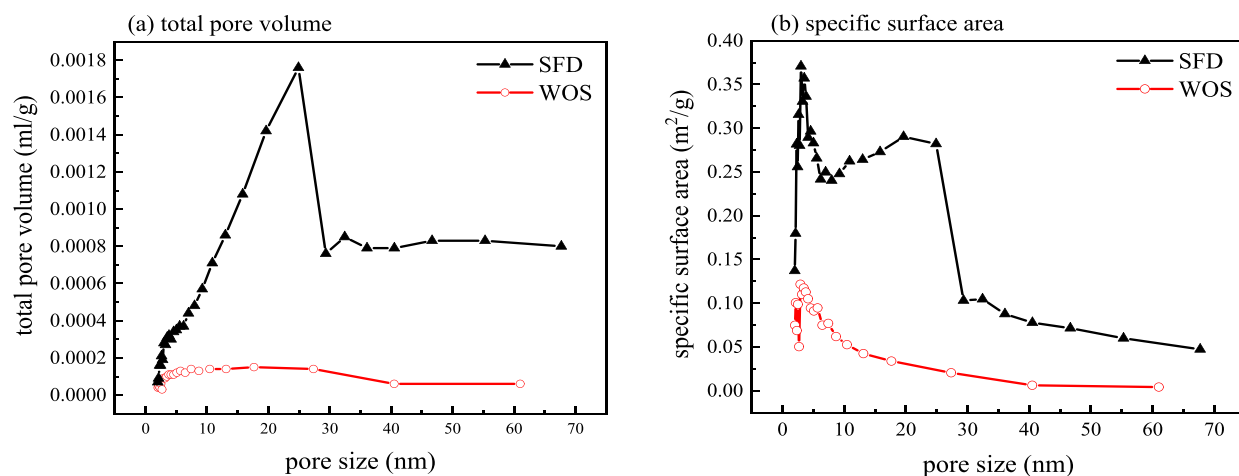


Figure 3. Pore structure distribution of SFD and WOS: (a) total pore volume and (b) the specific surface area.

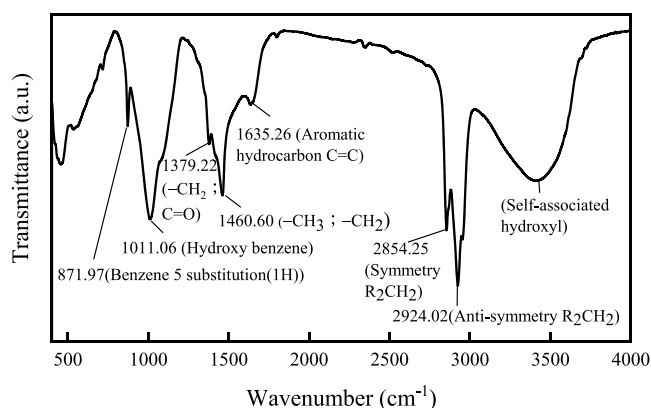


Figure 4. Infrared spectrogram of WOS.

decomposition of oils will absorb heat. There are obvious endothermic peaks corresponding to the three temperatures of 220, 350, and 430 °C, which means that the volatilization and decomposition temperatures of different components of oils are different. Two DSC endothermic peaks appear around 720 and 900 °C, which may be the high-temperature decomposition process of some inorganic compounds such as CaCO₃.⁴⁷ Figure 5b shows that the weight loss process of WOS in an oxygen atmosphere can also be divided into three stages, wherein the

evaporation of water and the decomposition of inorganic compounds are basically the same as those in an inert atmosphere; in the second stage, the sample rapidly loses weight at 220–320 °C and is accompanied by violent heat release. According to Table 2, the calorific value of WOS is 13,581 J/g, which is caused by the combustion reaction between organic matter and oxygen. In the co-heating process of WOS and coal, the heat released by the combustion of organic matter will compensate for the heat required for heating the inorganic matter in the additive and the heat required for coal pyrolysis. Therefore, the volatile matter is released earlier, promoting homogeneous and heterogeneous ignition of coal. This is an advantage that other ordinary inorganic additives do not possess.⁴⁸

The pulverized coal particles injected into the tuyere will be dispersed. At this time, the binding performance of additives and pulverized coal will affect the catalytic effect. Therefore, the dispersion of additives and pulverized coal is analyzed using the back-scattered electron of SEM. Because the complex mineral composition of pulverized coal will affect the identification of dispersed materials through the back-scattered electron signal, graphite powder with similar properties is used instead of pulverized coal as the matrix material. The SEM photographs of SFD and WOS mixed with graphite powder are presented in Figure 6. The darker and large irregular contours are graphite flakes, and the bright spots of freely distributed small particles

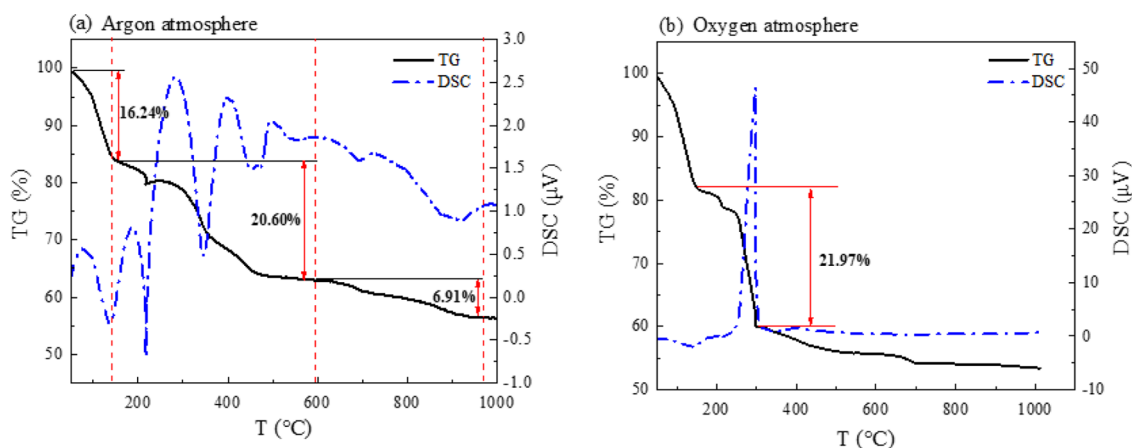


Figure 5. TG-DSC curves of WOS during heating under an (a) argon atmosphere and (b) an oxygen atmosphere.

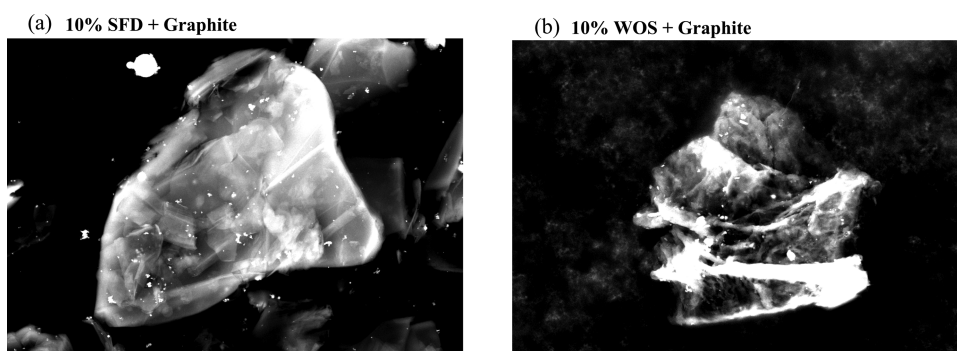


Figure 6. SEM images of SFD and WOS: (a) 10% SFD + graphite and (b) 10% WOS + graphite.

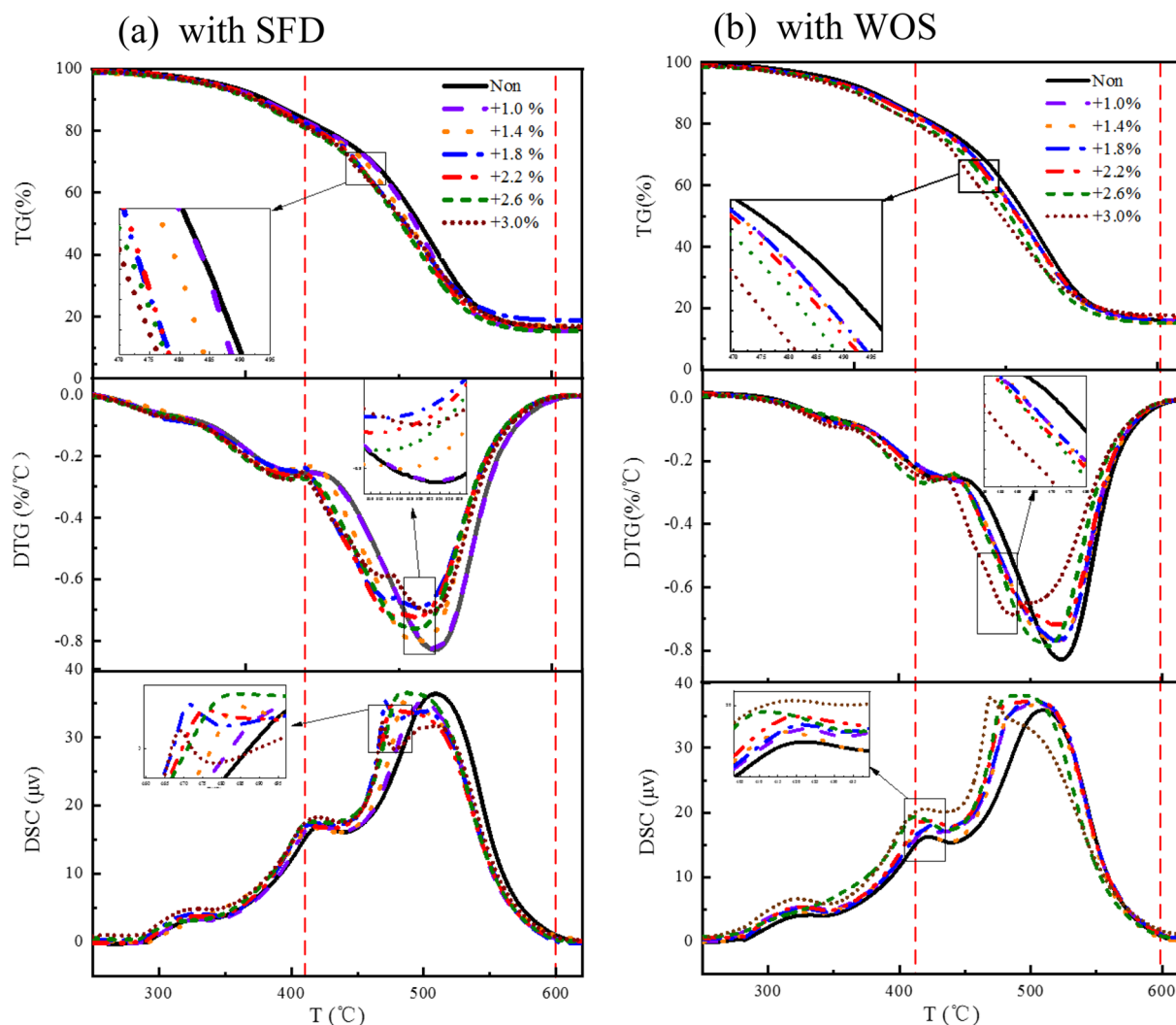


Figure 7. TG-DTG-DSC curves of pulverized coal and blend combustion: (a) SFD-mixed pulverized coal and (b) WOS-mixed pulverized coal.

are MDS. **Figure 6a** shows that after SFD is mixed with graphite powder, part of SFD adheres to the graphite; after mixing, the SFD is more uniformly distributed on the graphite powder. Compared with SFD, WOS adhered to the graphite powder in **Figure 6b** is equally uniform but with a relatively small quantity. This is due to the adhesion of organic matter in WOS, which renders the inorganic components in WOS less dispersed than SFD. The two types of MDS are mixed with pulverized coal and then injected into the BF under a high gas flow rate in the raceway of the tuyere;⁴⁹ this stable combination makes the

catalytic components in the MDS contact more closely with pulverized coal, which is more beneficial to the combustion and catalysis of pulverized coal.

3.2. Catalytic Effects of MDS on Pulverized Coal Combustion. The TG-DTG-DSC curves of the pulverized coal combustion process of two types of MDS with different ratios are demonstrated in **Figure 7**. According to the peak shape of the DTG and DSC curves, the combustion process of pulverized coal can be divided into two stages: (1) The volatile escaping and homogeneous combustion stage (260–410 °C);

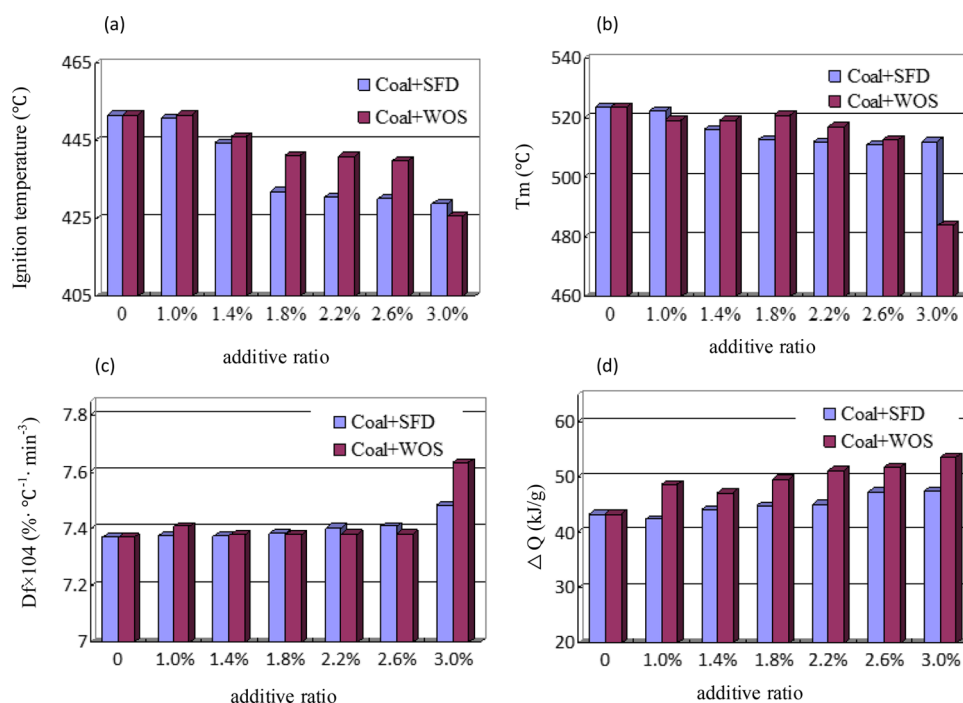


Figure 8. Combustion characteristic parameters of pulverized coal and blend combustion: (a) ignition temperature, (b) T_m , (c) D_f and (d) ΔQ .

the organic components in coal undergo a small amount of easy-to-break small molecular side-chain pyrolysis at about 320 °C, perform a fast thermal decomposition process at 350–410 °C, and react with oxygen in the atmosphere with rapid heat release. The weight loss of pulverized coal in this stage is about 10%, which is basically consistent with the volatile matter content of the coal in industrial analysis. (2) The second stage is the char combustion stage (410–600 °C). As the temperature rises, the char reaches the ignition temperature and burns rapidly. The combustion rate reaches the maximum near 520, then the combustion rate gradually decreases, and the char burns out near 600 °C.

Figure 7a shows that during the pyrolysis stage, the DSC curve of pulverized coal added with SFD hardly changes, and only fluctuates near the original curve of pulverized coal, indicating that SFD has no obvious catalytic effect on the pyrolysis stage of pulverized coal. In the char combustion stage, after adding SFD, the entire thermal analysis curve shifts toward the low-temperature area. From the DTG curve, it is found that the effect of additives on the reaction rate is mainly reflected in the reduction of temperature corresponding to the maximum combustion rate, but it does not increase the maximum combustion rate value; however, the DSC curve reveals that both the heat flow rate and its corresponding temperature are affected by additives and the combustion efficiency is improved.

According to Figure 7b, when WOS is added, the DSC curve of pulverized coal at the same temperature in the pyrolysis stage rises, and as the ratio of addition increases, the increment of heat flow also becomes larger. Notably, before 320 °C, additives have little effect on TG and DTG curves but have a greater effect on DSC. This is because at this stage, the rapid combustion of organic matter in WOS (see Figure 5b) increases heat release but has little effect on the breakage of chemical bonds of the pulverized coal itself. The difference is that the heat release rate and weight loss rate of pulverized coal in the rapid pyrolysis stage (350–410 °C) simultaneously increase, but the organic matter combustion in WOS almost ends. Thus, this change is due to the

variation in the pulverized coal's own organic matter thermal decomposition and the combustion behavior under the action of additives. In the char combustion stage, after adding WOS, the curve is similar to the curve of adding SFD at this stage. The entire DTG curve moves toward the lower temperature, and the DSC curve is obviously lifted. Compared to the results of samples with SFD, the DTG and DSC curves of samples with added WOS have a more obvious moving trend. The influence of the two types of MDS on the reaction rate is reflected in the decrease of the temperature corresponding to the maximum combustion rate and the increase in the heat flow rate.

The characteristic parameters of the pulverized coal combustion process with the added MDS are presented in Figure 8. Figure 8a shows that the ignition temperature of pulverized coal with SFD added decreases. When the ratio is greater than 1.8%, the degree of ignition temperature reduction is small. The ignition temperature of pulverized coal also drops with the increase in the ratio after adding WOS. With the increase in the ratio of addition, the degree of reduction of the ignition temperature increases. On the whole, the ignition temperature of pulverized coal with SFD is reduced to a greater extent, and the improvement in the ignition performance of SFD on pulverized coal is superior to that of WOS.

Figure 8b exhibits the temperature change corresponding to the maximum combustion rate of pulverized coal with two types of singular MDS. After adding SFD, the temperature corresponding to the maximum combustion rate of pulverized coal demonstrates a decreasing trend. As the ratio of addition increases, there is little difference in the decreasing trend. The temperature corresponding to the maximum combustion rate of pulverized coal with WOS also drops with the increase in the ratio. The sample with 3% SFD decreases by 11.47 °C compared with pulverized coal; moreover, compared with pulverized coal, the sample with 3% WOS experiences the largest reduction of 39.57 °C, indicating that both types of MDS make the time corresponding to the fast combustion stage advance. When the ratio is 3%, WOS has a greater impact on pulverized coal.

Figure 8c reveals that the burnout index D_f of pulverized coal increases after adding SFD or WOS. Because the catalytic components in the two types of MDS make pulverized coal come in closer contact with the surrounding oxygen,⁵⁰ the residue of unburned pulverized coal is reduced such that the combustion of pulverized coal is more complete. When the ratio of addition is less than 3%, the increasing trend of burnout index is not evident. When the ratio of addition is 3%, D_f significantly increases, and the improvement effect of WOS on the burnout index of pulverized coal is greater than that of the sample with SFD.

According to the DSC curve and eq 1, the calorific value (ΔQ) of the samples during the combustion process is calculated as shown in Figure 8d. After adding SFD, the calorific value of pulverized coal becomes larger with the increase in the ratio of addition. After adding WOS, the heat release of pulverized coal also grows with the increasing ratio. Overall, the heat release of the sample with the same ratio of WOS is more evident, and the heat release of pulverized coal with 3% WOS increases by 23.77%. This is because the self-combustion of organic matter in WOS during the pyrolysis stage will increase the heat release, and the organic matter in WOS plays a dominant role in the pyrolysis stage; thus, the heat released by pulverized coal after adding WOS is greater than that when SFD is added.

In summary, the enhanced combustion effect of SFD on pulverized coal is mainly manifested in the reduction of the ignition temperature of pulverized coal and the temperature corresponding to the maximum combustion rate. Only when the amount of addition in the two types of MDS is large will it significantly impact the burnout index of pulverized coal.

3.3. Analysis of the Enhanced Combustion Mechanism. The influence of additives on pulverized coal combustion can be divided into the devolatilization stage and char combustion stage. To explore the effect of adding MDS on the pyrolysis and combustion process of pulverized coal, the pulverized coal and the mixed samples with SFD and WOS, respectively, added are pyrolyzed in a tube furnace to prepare char and test the specific surface area and carbon chemical structure. The pore structure parameter values of char and their distribution with pore size are presented in Table 4 and Figure 9,

Table 4. Pore Structure Values of the Char Using the N_2 Adsorption Method

sample	specific surface area (m ² /g)	total pore volume (cm ³ /g)	average pore size (nm)
char-non additive	13.424	0.017	4.930
char-10%SFD	15.206	0.018	4.663
char-10% WOS	21.824	0.024	4.184

respectively. Compared with the value of the specific surface area of the char-non additive, the value increases by 13.33% after adding SFD, whereas the value increases by 62.57% after adding WOS. The addition of MDS significantly enlarges the specific surface area of the char and increases the total pore volume.

Figure 9a shows that the pore diameters of the three types of char are similar, all in the range of 3–70 nm, and most of them are mesoporous. Figure 9b shows that the pores below a 30 nm size of the three types of char all contribute to a large specific surface area. When the pore size is below 3 nm, compared with the char-non additive, the samples with two types of MDS have larger specific surface areas. The trend of change after adding

WOS is the most obvious. When the pore size is in the range of 3–10 nm, the specific surface area of the char is larger; as a whole, the specific surface area of the samples after adding MDS increases, and the smaller pore size contributes more to the specific surface area. It is concluded that the MDS develops the micropores and smaller mesopores of the char, and the specific surface area increases. This is because the organic matter combustion in WOS in the early pyrolysis stage releases substantial heat, thereby promoting the escape of volatile matters. Pulverized coal absorbs part of the heat to increase its own internal energy, enhancing the char performance and accelerating the achievement of the volatile matter combustion temperature; furthermore, the calorific value needed to reach the ignition temperature is guaranteed.⁵¹ In the pyrolysis stage, WOS has a dominant effect on pulverized coal; thus, the specific surface area of the sample with WOS is greater than that of SFD. Moreover, the Fe₂O₃ in the MDS may combine with the functional groups of the pulverized coal structure to form various new and more reactive chemical bonds, such as C–O–Fe and C–O–O–Fe, which pyrolyzes again and results in the release of more CO₂, CO, and CH₄ gases. During the release of the gases, the pores on the surface of the char are more developed, thereby enlarging the specific surface area of the samples and making the inorganic catalytic components in MDS make closer contact with pulverized coal,⁵⁰ which prepares a good gas–solid reaction interface for subsequent char combustion.⁵²

Figure 10 shows the Raman analysis results of three types of char. The characteristic peaks obtained by the peak fitting of the Raman spectrum are shown in Figure 13a. There are D1 band (1350 cm⁻¹), D2 band (1620 cm⁻¹), D3 band (1350 cm⁻¹), D4 band (1150 cm⁻¹), and G band (1580 cm⁻¹). The D1 band belongs to a relatively large aromatic ring structure, the D2 band represents the irregular arrangement of the carbon structure, the D3 band is an amorphous carbon structure, the D4 peak is the aliphatic or polyene-like structure, and the G band represents an ideal graphite structure.⁵³ A_G/A_{All} is used to characterize the graphitization degree of char. The higher value implies a greater graphitization degree of char.⁵⁴ A_{D1}/A_G characterizes the degree of disorder of char. The larger value represents a higher ratio of the defect structure of semicoke and better reactivity of the char.^{55,56} According to Figure 10b, the A_G/A_{All} of pulverized coal decreases after adding MDS. This value of char-10%SFD decreases by 14.63% and that of char-10%WOS decreases by 20.28%, indicating that the addition of two types of MDS reduces the graphitization structure of char-non additive, rendering the char structure disordered. The ratio of A_{D1}/A_G of the sample increases after adding MDS, and the value increases more evidently with the addition of WOS, which reflects that MDS can make pulverized coal disordered or increase the defective structure during pyrolysis. This is because the inorganic components Fe₂O₃ and CaO in MDS catalyze the pyrolysis of pulverized coal, increasing disorder and the defect structure of the obtained char.⁵⁰ Thus, the addition of MDS renders the carbon chemical structure of char more disordered and defective, and the regular graphitization of the structure is reduced, increasing the reactivity of char in the subsequent combustion stage.

According to the bulk diffusion theory, in the char combustion stage, the catalytic components (Fe₂O₃ and CaO) in SFD and WOS promote the dissolution of carbon atoms at the catalyst–carbon interface, enter the catalyst, and gradually diffuse and form a concentration gradient. When the carbon atoms reach the

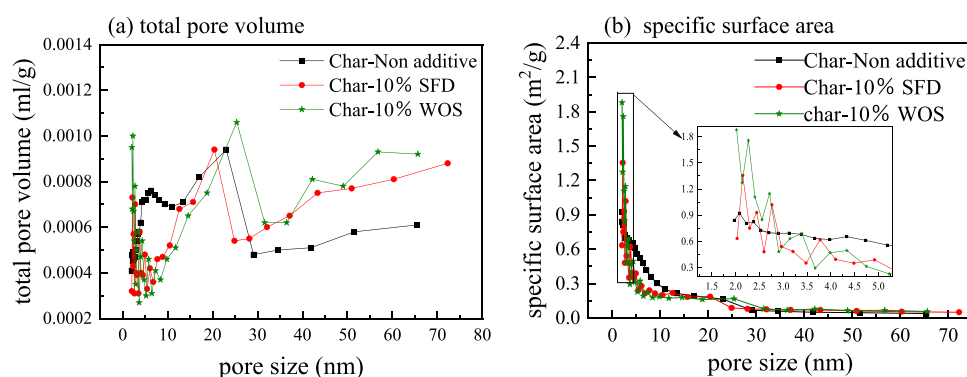


Figure 9. Pore structure distribution of chars: (a) pore volume and (b) specific surface area.

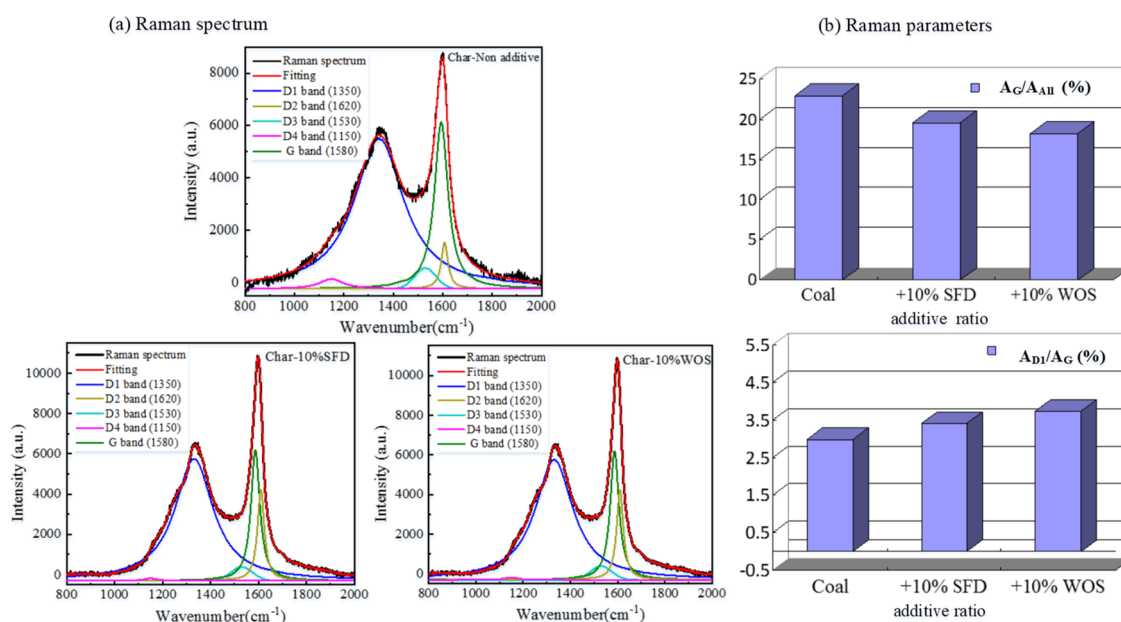


Figure 10. Raman analysis of chars: (a) peak fitting of the Raman spectrum and (b) the variation of characteristic parameters.

catalyst–gas interface, they react with the oxygen adhered to the catalyst surface.^{57,58} The addition of MDS in the pyrolysis stage increases disorder and defects of the char's carbon chemical structure, which increases reaction active points on char, making the carbon–oxygen reaction at the catalyst–gas interface more likely to react and the reaction more complete. Additionally, the inorganic component Fe_3O_4 in MDS oxidizes and releases heat, which promotes the complete combustion of pulverized coal and increases the heat release of the sample. Therefore, the addition of MDS will reduce the temperature corresponding to the maximum combustion rate of pulverized coal and increase the heat release of the combustion reaction.

Our previous research presents that Fe_2O_3 and CaO , the main catalytic components usually contained in MDS, may sinter at a certain temperature, causing catalyst deactivation. Figure 11³⁴ combines the effect of catalytic components on graphite combustion with the Fe_2O_3 – CaO binary phase diagram; using this diagram, the occurrence of sintering catalytic deactivation between calcium oxide and iron oxide in the MDS can be determined. Combining the Fe_2O_3 – CaO ratio and burnout index of the test sample, the result is marked in the red dashed box in the figure. The samples except the char-non additive are inside the $2\text{CaO}\cdot\text{Fe}_2\text{O}_3 + \text{CaO}$ zone. In this zone, all catalysts demonstrate satisfied catalytic activity for the combustion of

graphite; hence, the catalytic activities of two types of MDS, SFD, and WOS, on the combustion of pulverized coal are favorable.

When the catalyst is added, there is an optimal adding ratio. When the addition amount of the catalyst is less than the optimal ratio, the catalyst cannot provide enough catalytic active points. There is a catalytic effect but not the best. When the addition amount of the catalyst is larger than the optimal ratio, because the catalyst covers the surface of fuel particles, it blocks numerous pores and reduces the carbon–oxygen contact area, intensifying gas diffusion resistance during the combustion process, which is not conducive to the combustion reaction.⁵⁹ The ignition temperature of pulverized coal and the temperature corresponding to the maximum combustion rate decrease with the increase in the ratio of MDS, and the burnout index and heat release increase with the increase in the ratio of MDS. This is because the addition ratio of the two types of MDS does not reach the optimal addition ratio of the catalyst.⁶⁰

To further explore the effect of adding MDS on the combustion kinetics, the combustion process of the pulverized coal and the mixed samples with SFD and WOS, respectively, added according to eq 8 is calculated and fitted, as shown in Figure 12. The kinetic parameters obtained are listed in Table 5. The activation energy of the samples added with MDS has

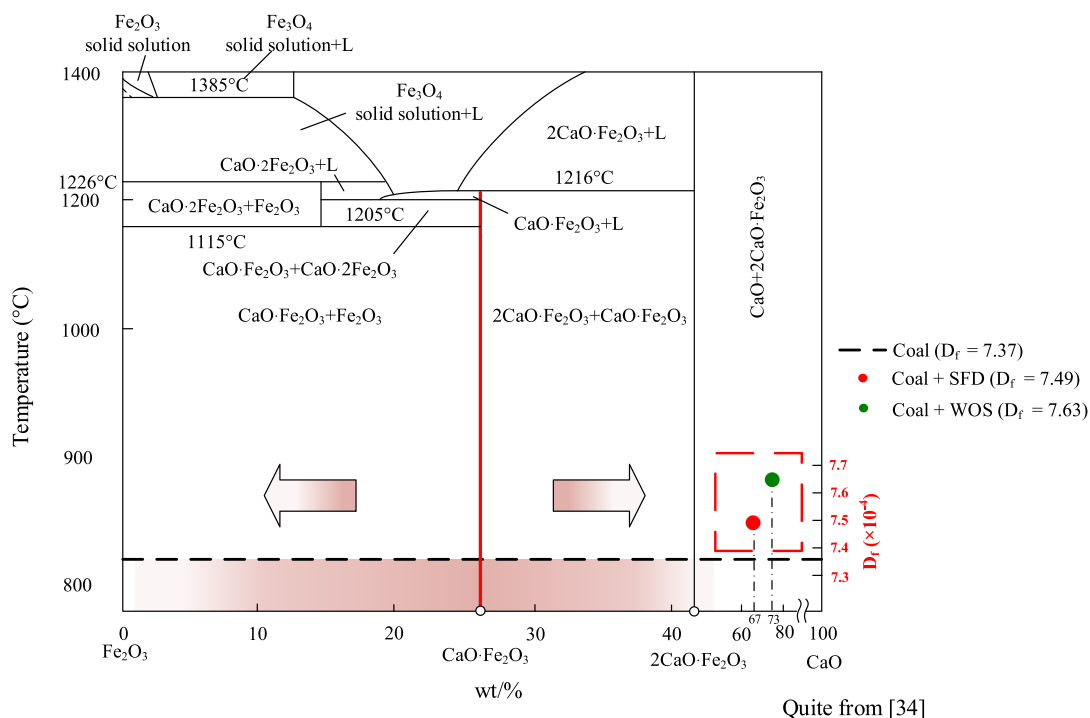


Figure 11. Catalytic effects of the investigated samples overlaid on the Fe_2O_3 – CaO binary phase diagram (dotted line represents the burnout index of coal, and the red-shaded area represents the Fe–Ca sintering and inhibition ratio).

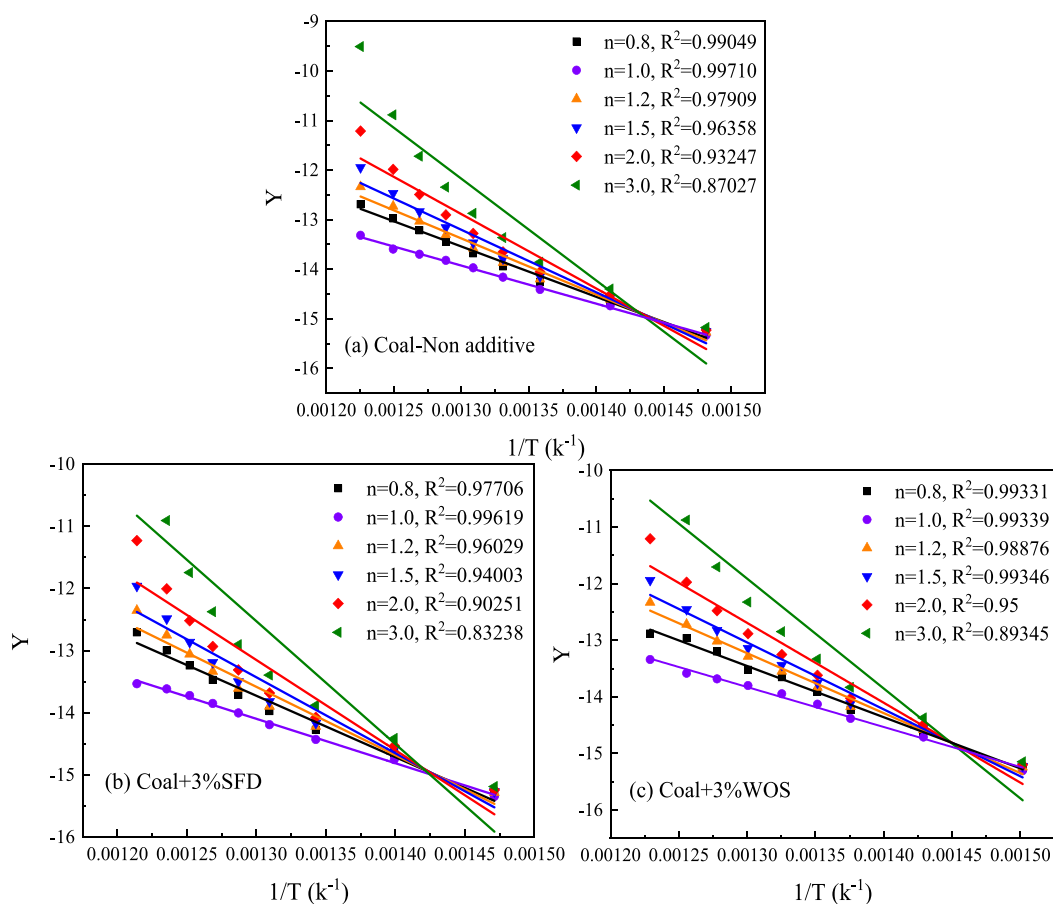


Figure 12. Linear fitting diagram of combustion kinetics of blend combination.

reduced. After adding SFD, the activation energy of pulverized coal reduces by 7.14%, and after adding WOS, the activation

energy of pulverized coal combustion reduces by 8.12%. On the one hand, the addition of WOS and SFD accelerates the

Table 5. Kinetic Parameters of Blends

add ratio	temperature range (°C)	<i>E</i> (kJ/mol)	<i>A</i> (min ⁻¹)	<i>n</i>	<i>R</i> ²
coal	451.62–586.72	63.91	2261.03	1	0.99710
coal + 3% SFD	428.81–584.65	59.35	1019.85	1	0.99619
coal + 3% WOS	421.18–577.53	58.72	866.33	1	0.99369

pyrolysis of pulverized coal to form char with developed porosity and a disordered carbon structure, reducing the energy required for the combustion of char. On the other hand, the inorganic catalytic components (Fe₂O₃ and CaO) in MDS have numerous lattice defects and molecular holes, which can accelerate the adsorption of oxygen on the surface of the catalyst and the diffusion of carbon atoms in the catalyst under the oxygen environment. Therefore, the activation energy was decreased and the combustion reaction rate was accelerated. It is easier for the combustion reaction to occur in this scenario than before adding MDS.

In summary, the strengthened mechanism of pulverized coal combustion by MDS can be described in Figure 13. (1) Devolatilization stage: the organic components in WOS burn out to release heat to promote the escape of volatiles in pulverized coal. Simultaneously, the inorganic catalytic components in MDS catalyze the pyrolysis of pulverized coal such that the pores on the surface of char are more developed and the specific surface area increases. Owing to the addition of MDS, the carbon chemical structure of char becomes more disordered during the pyrolysis of pulverized coal, and the defect structure of char increases. (2) Char combustion stage: the disordered structure of char resulting from the addition of MDS provides more active points; further, the more developed pore structure of char provides more specific surface area, both of which enhance oxygen adsorption. The catalytic effect of the catalyst on the combustion of char is further improved, and the activation energy of the combustion reaction is reduced. Moreover, the inorganic component Fe₃O₄ and organic matter in MDS oxidize and release heat, accelerating the diffusion rate of carbon atoms in the catalyst and promoting the carbon–oxygen reaction.

4. CONCLUSIONS

- (1) The particle sizes of the two types of MDS are extremely small, and the pores are developed. They are evenly dispersed after being mixed with pulverized coal and are stably combined with it. The heat released by organic matter combustion will compensate for the heat required for the heating of inorganic matters in the additive and the pyrolysis of the pulverized coal, thereby advancing escape of volatile in pulverized coal and promoting homogeneous ignition.
- (2) The catalytic effect of SFD on pulverized coal is mainly reflected in reducing the ignition temperature of pulverized coal and the temperature corresponding to the maximum combustion rate.
- (3) The combustion of organic components in MDS promotes the escape of volatile matters of pulverized coal. The inorganic catalytic components will catalyze the pyrolysis of pulverized coal, making pores on the surface of char more developed, the specific surface area larger, the carbonization structure more disordered, and the defective structure of char increase, which provide a larger specific surface area, enhancing the catalytic effect of the catalyst on the combustion of char.
- (4) There is no sintering catalyst deactivation phenomenon under the ratio of inorganic compounds in SFD and WOS. The inorganic catalytic components in MDS will accelerate the rate of the combustion reaction and reduce the activation energy of the reaction.

AUTHOR INFORMATION

Corresponding Author

Chong Zou – School of Metallurgical Engineering, Xi'an University of Architecture and Technology, Xi'an 710055, China; orcid.org/0000-0003-4734-361X; Email: zouchong@xauat.edu.cn

Authors

Yu Wang – School of Metallurgical Engineering, Xi'an University of Architecture and Technology, Xi'an 710055, China

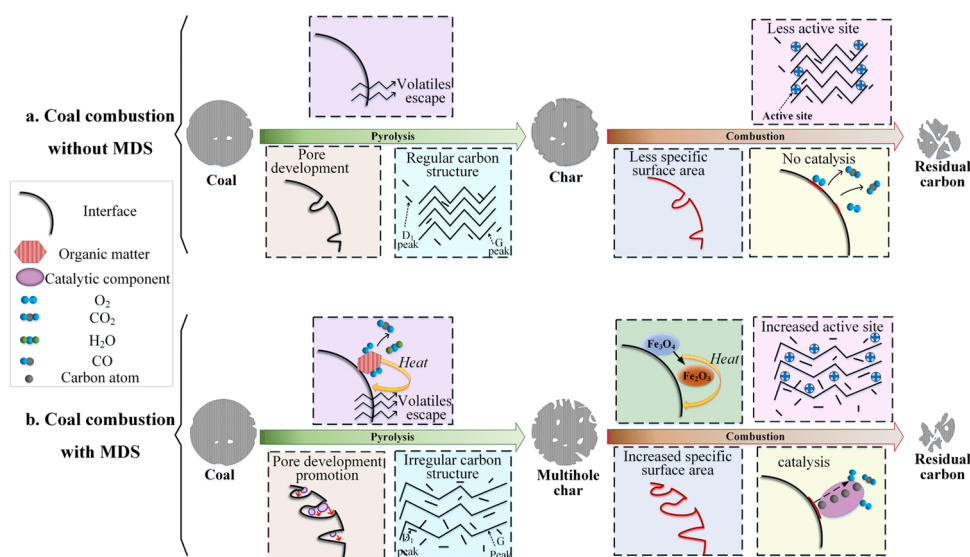


Figure 13. Mechanism diagram of enhanced combustion of MDS.

Junxue Zhao – School of Metallurgical Engineering, Xi'an University of Architecture and Technology, Xi'an 710055, China

Fei Wang – School of Metallurgical Engineering, Xi'an University of Architecture and Technology, Xi'an 710055, China

Complete contact information is available at:
<https://pubs.acs.org/10.1021/acsomega.1c02554>

Notes

The authors declare no competing financial interest.

ACKNOWLEDGMENTS

The authors thank the Natural Science Foundation Project of China (nos. 51704224 and 51904223) and the Shaanxi Provincial Key Research and Development Program (2021GY-128 and 2020GY-229) for funding this research.

REFERENCES

- (1) Xufang, P. Reasonable Recycle Utilization Technology of Iron Containing Dust Slime of Metallurgical Industry. *Modern Mining* **2010**, *5*, 57–59.
- (2) Tian, W.; Yue, C.; Pen, B. Analysis of the Characteristics and Disposal Technology of Metallurgical Dust. *Conserv. Util. Miner. Resour.* **2019**, *39*, 105–110.
- (3) Leimalm, U.; Lundgren, M.; Ökvist, L. S.; Björkman, B. Off-gas Dust in an experimental blast furnace. *ISIJ Int.* **2010**, *50*, 1560–1569.
- (4) Borrego, A. G.; Osório, E.; Casal, M. D.; Vilela, A. C. F. Coal char combustion under a CO₂-rich atmosphere: Implications for pulverized coal injection in a blast furnace. *Fuel Process. Technol.* **2008**, *89*, 1017–1024.
- (5) Helle, H.; Helle, M.; Saxén, H.; Pettersson, F. Optimization of top gas recycling conditions under high oxygen enrichment in the blast furnace. *ISIJ Int.* **2010**, *50*, 931–938.
- (6) Terpák, J.; Dorčák, L.; Košťál, I.; Pivka, L. Reduction of Costs of Iron Production by Changing Parameters of the Mixed Blast-Furnace Wind. *Metalurgija* **2010**, *49*, 79.
- (7) Zhu, C.; Jiang, Y.; Ding, H. Research progress of the coal-combustion catalysts in China. *Goal qual. technol.* **2010**, *4*, 41–44.
- (8) Zhao, J.; Wang, H.; Yang, Y.; Du, H.; Song, G. Impact of Pulverized Coal Preheating on Coal Combustion Behavior in Pulverized Coal Injection of Blast Furnace. *Chin. J. Process Eng.* **2011**, *11*, 606–612.
- (9) Wang, S. J.; Wu, F.; Zhang, G.; Zhu, P.; Wang, Z. Y.; Huang, C. J.; Chen, S. T. Research on the combustion characteristics of anthracite and blended coal with composite catalysts. *J. Energy Inst.* **2014**, *87*, 96–101.
- (10) Senk, D.; Gudenau, H. W.; Geimer, S.; Gorbunova, E. Dust injection in iron and steel metallurgy. *ISIJ Int.* **2006**, *46*, 1745–1751.
- (11) Ökvist, L. S.; Cang, D.; Zong, Y.; Bai, H. The effect of BOF slag and BF flue dust on coal combustion efficiency. *ISIJ Int.* **2004**, *44*, 1501–1510.
- (12) Chong, Z.; Liangying, W.; Chengbin, Y.; Shengfu, Z.; Chenguang, B.; Xiuqin, T. Effect of Iron Containing Metallurgical Byproducts on Pulverized Coal Combustion Efficiency. *3rd International Symposium on High-Temperature Metallurgical Processing*; John Wiley & Sons, Inc.: Hoboken, NJ, USA, 2012, 1–6.
- (13) Chong, Z.; Liangying, W.; Shengfu, Z.; Chenguang, B.; Xiuqin, T. Effect of Iron Containing Metallurgical Byproducts on Pulverized Coal Combustion Efficiency. In *3rd International Symposium on High-Temperature Metallurgical Processing*; John Wiley & Sons, Inc.: Hoboken, NJ, USA, 2012, 439–446, DOI: 10.1002/9781118364987.ch53.
- (14) Zou, C.; Zhao, J. Investigation of iron-containing powder on coal combustion behavior. *J. Energy Inst.* **2017**, *90*, 797–805.
- (15) Zou, C.; Wu, H.; Zhao, J.; Li, X. Effects of dust collection from converter steelmaking process on combustion characteristics of pulverized coal. *Powder Technol.* **2018**, *332*, 70–78.
- (16) Liu, J.; Jiang, X.; Han, X. Devolatilization of oil sludge in a lab-scale bubbling fluidized bed. *J. Hazard. Mater.* **2011**, *185*, 1205–1213.
- (17) Ramaswamy, B.; Kar, D. D.; De, S. A study on recovery of oil from sludge containing oil using froth flotation. *J. Environ. Manage.* **2007**, *85*, 150–154.
- (18) Zhou, L.; Jiang, X.; Liu, J. Characteristics of oily sludge combustion in circulating fluidized beds. *J. Hazard. Mater.* **2009**, *170*, 175–179.
- (19) Qin, L.; Han, J.; He, X.; Zhan, Y.; Yu, F. Recovery of energy and iron from oily sludge pyrolysis in a fluidized bed reactor. *J. Environ. Manage.* **2015**, *154*, 177–182.
- (20) Zubaidy, E. A. H.; Abouelnasr, D. M. Fuel recovery from waste oily sludge using solvent extraction. *Process Saf. Environ. Prot.* **2010**, *88*, 318–326.
- (21) Li, C. T.; Lee, W. J.; Mi, H. H.; Su, C. C. PAH emission from the incineration of waste oily sludge and PE plastic mixtures. *Sci. Total Environ.* **1995**, *170*, 171–183.
- (22) Sankaran, S.; Pandey, S.; Sumathy, K. Experimental investigation on waste heat recovery by refinery oil sludge incineration using fluidised-bed technique. *Journal of Environmental Science and Health Part A.* **1998**, *33*, 829–845.
- (23) Biswal, B. K.; Tiwari, S. N.; Mukherji, S. Biodegradation of oil in oily sludges from steel mills. *Bioresour. Technol. Rep.* **2009**, *100*, 1700–1703.
- (24) Liu, W.; Luo, Y.; Teng, Y.; Li, Z.; Christie, P. Prepared bed bioremediation of oily sludge in an oilfield in northern China. *J. Hazard. Mater.* **2009**, *161*, 479–484.
- (25) Shahraki, S.; Miri, M.; Motahari-Nezhad, M. Experimental analysis of pyrolysis of sewage sludge. *Energy Sources, Part A* **2018**, *40*, 2037–2043.
- (26) Schmidt, H.; Kaminsky, W. Pyrolysis of oil sludge in a fluidised bed reactor. *Chemosphere* **2001**, *45*, 285–290.
- (27) Karamalidis, A. K.; Voudrias, E. A. Release of Zn, Ni, Cu, SO₄²⁻ and CrO₄²⁻ as a function of pH from cement-based stabilized/solidified refinery oily sludge and ash from incineration of oily sludge. *J. Hazard. Mater.* **2007**, *141*, 591–606.
- (28) Yao, H.; Naruse, I. Behavior of lead compounds during municipal solid waste incineration. *Proc. Combust. Inst.* **2009**, *32*, 2685–2691.
- (29) Hejazi, R. F.; Husain, T.; Khan, F. I. Landfarming operation of oily sludge in arid region—human health risk assessment. *J. Hazard. Mater.* **2003**, *99*, 287–302.
- (30) Zhao, Z.; Li, W.; Qiu, J.; Li, B. Catalytic effect of Na–Fe on NO–char reaction and NO emission during coal char combustion. *Fuel* **2002**, *81*, 2343–2348.
- (31) Cui, X.; Zhang, X.; Feng, Y.; Wang, G.; Yang, M.; Gao, H.; Luo, W. Effect of partial substitution of Ca in LaMnO₃ on coal catalytic combustion. *J. Therm. Anal. Calorim.* **2013**, *112*, 719–726.
- (32) Cheng, J.; Zhou, F.; Xuan, X.; Liu, J.; Zhou, J.; Cen, K. Cascade chain catalysis of coal combustion by Na–Fe–Ca composite promoters from industrial wastes. *Fuel* **2016**, *181*, 820–826.
- (33) Gong, X.; Guo, Z.; Wang, Z. Anthracite combustion catalyzed by Ca–Fe–Ce series catalyst. *J. Fuel Chem. Technol.* **2009**, *37*, 421–426.
- (34) Zou, C.; Kang, Y.; Wang, W.; Wang, Y.; Shi, R. Effects of Fe₂O₃–CaO Interactions in Metallurgical Dust on Its Catalytic Activity for the Carbon–Oxygen Reaction. *Energy Fuels* **2019**, *33*, 11830–11840.
- (35) Chavda, R.; Mahanwar, P. Effect of inorganic and organic additives on coal combustion: a review. *Int. J. Coal Prep. Util.* **2021**, *41*, 749–766.
- (36) Wagloehner, S.; Baer, J. N.; Kureti, S. Structure–activity relation of iron oxide catalysts in soot oxidation. *Appl. Catal., B* **2014**, *147*, 1000–1008.
- (37) Tomita, A. Catalysis of carbon–gas reactions. *Catal. Surv. Jpn.* **2001**, *5*, 17–24.
- (38) Lobo, L. S.; Carabineiro, S. A. C. Kinetics and mechanism of catalytic carbon gasification. *Fuel* **2016**, *183*, 457–469.

- (39) Wagloehner, S.; Kureti, S. Study on the mechanism of the oxidation of soot on Fe_2O_3 catalyst. *Applied Catalysis B Environmental*. **2012**, *125*, 158–165.
- (40) Keep, C. W.; Terry, S.; Wells, M. Studies of the nickel-catalyzed hydrogenation of graphite. *J. Catal.* **1980**, *66*, 451–462.
- (41) Gong, X.; Guo, Z.; Wang, Z. Effect of K_2CO_3 and Fe_2O_3 on combustion reactivity of pulverized coal by thermogravimetry analysis. *J. Chem. Technol. Biotechnol.* **2009**, *37*, 42–47.
- (42) Kang, Y.; Zou, C.; Zhao, J.; He, J.; Ma, C.; Zhang, X. Microstructure characteristics of semi-coke under different pyrolysis processes and its influence on combustion performance. *J. Iron Steel Res.* **2019**, *31*, 601–611.
- (43) Zou, C.; Wen, L.; Zhang, S.; Bai, C.; Yin, G. Evaluation of catalytic combustion of pulverized coal for use in pulverized coal injection (PCI) and its influence on properties of unburnt chars. *Fuel Process. Technol.* **2014**, *119*, 136–145.
- (44) Coats, A. W.; Redfern, J. P. Kinetic parameters from thermogravimetric data. *Nature* **1964**, *201*, 68–69.
- (45) Gao, Z.; Su, C.; Li, N.; Chun, T.; Yu, Z.; Liu, H. Preparation of Ca-Fe oxygen carrier using metallurgical dust. *J. Iron Steel Res.* **2018**, *30*, 782–788.
- (46) Jirasripongpun, K. The characterization of oil-degrading microorganisms from lubricating oil contaminated (scale) soil. *Let. Appl. Microbiol.* **2002**, *35*, 296–300.
- (47) Li, M.; Chi, K.; Gao, S.; Wang, Y.; Huang, X. Production status quo and development trend of lube oil base oil. *Refin. Chem. Ind.* **2009**, *4*, 5–8.
- (48) Guo, X.-Z.; Wei, G.; Zhou, Y.-p.; Ma, Z.-f.; Ding, Z.-m.; Shemn, F.-m. Effect of MgO addition on burnout rate of pulverized coal for blast furnace injection. *Iron Steel/Gangtie* **2011**, *46*, 7–9.
- (49) Zhuo, Y.; Shen, Y. Three-dimensional transient modelling of coal and coke co-combustion in the dynamic raceway of ironmaking blast furnaces. *Appl. Energy* **2020**, *261*, 114456.
- (50) Gong, X.; Guo, Z.; Wang, Z. Variation of char structure during anthracite pyrolysis catalyzed by Fe_2O_3 and its influence on char combustion reactivity. *Energy Fuels* **2009**, *23*, 4547–4552.
- (51) Deng, J.; Wang, K.; Zhang, Y.; Yang, H. Study on the kinetics and reactivity at the ignition temperature of Jurassic coal in North Shaanxi. *J. Therm. Anal. Calorim.* **2014**, *118*, 417–423.
- (52) Wang, Z.; Zhao, Y.; Sun, R.; Li, Y.; Ren, X.; Xu, J. Effect of reaction conditions on the evolution of surface functional groups in $\text{O}_2/\text{H}_2\text{O}$ combustion process of demineralized coal char. *Fuel Process. Technol.* **2019**, *195*, 106144.
- (53) Zhu, Y.; Zhao, X.; Gao, L.; Chen, J.; Lv, J.; Lai, S. Quantitative Study of the Microcrystal Structure on Coal Based on Needle Coke with Curve-Fitted of XRD and Raman Spectrum. *Spectrosc. Spectral Anal.* **2017**, *37*, 1919–1924.
- (54) Wang, B.; Sun, L.; Su, S.; Xiang, J.; Hu, S.; Fei, H. Char structural evolution during pyrolysis and its influence on combustion reactivity in air and oxy-fuel conditions. *Energy Fuels* **2012**, *26*, 1565–1574.
- (55) Li, X.; Hayashi, J.-i.; Li, C.-Z. Volatilisation and catalytic effects of alkali and alkaline earth metallic species during the pyrolysis and gasification of Victorian brown coal. Part VII. Raman spectroscopic study on the changes in char structure during the catalytic gasification in air. *Fuel* **2006**, *85*, 1509–1517.
- (56) Zhang, Y.; Zhu, J.; Lyu, Q.; Liu, J.; Pan, F. Coke generation and conversion behavior of pulverized coal combustion. *J. Energy Inst.* **2020**, *93*, 2096–2107.
- (57) Lobo, L. Catalytic carbon gasification: review of observed kinetics and proposed mechanisms or models-highlighting carbon bulk diffusion. *Catalysis Reviews*. **2013**, *55*, 210–254.
- (58) Schneider, C.; Walker, S.; Phounglamcheik, A.; Umeki, K.; Kolb, T. Effect of calcium dispersion and graphitization during high-temperature pyrolysis of beech wood char on the gasification rate with CO_2 . *Fuel* **2021**, *283*, 118826.
- (59) Zhang, H.; Guo, Z. C.; Wang, Z.; Xu, D. P. Effects of Catalysts on Combustion of Pulverized Coal by Synthetical Thermo-gravimetric Analysis. *Chin. J. Process Eng.* **2007**, *7*, 1154–1158.
- (60) Dahou, T.; Defoort, F.; Khiari, B.; Labaki, M.; Dupont, C.; Jeguirim, M. Role of inorganics on the biomass char gasification reactivity: A review involving reaction mechanisms and kinetics models. *Renewable Sustainable Energy Rev.* **2021**, *135*, 110136.